Journal of
Renewable Energy Research and Applications (RERA)

Vol. 6, No 1, 2024, 105- 124 *DOI: 10.22044/rera.2024.13663.1258*

A Novel Non-linear Analytical Solution for Thermal Performance of a Photovoltaic Module in Vicinity of Phase-changing Materials

A. Mahdavi[1], M. Farhadi[1*], M. Gorji-Bandpy[1] and A. Mahmoudi[2]

1. Faculty of Mechanical Engineering, Babol Noshirvani University of Technology, Shariati, Babol, Iran.
2. Department of Thermal and Fluid Engineering, University of Twente, Enschede, the Netherlands.

Received Date 28 September 2023; Revised Date 02 January 2024; Accepted Date 02 January 2024
**Corresponding author: mfarhadi@nit.ac.ir (M. Farhadi)*

Abstract
Regulating the operating temperature of photovoltaic (PV) systems is essential for their longevity. An efficient passive cooling method involves the incorporation of Phase Change Materials (PCMs). In this study, a novel non-linear analytical solution is employed to investigate the melting and solidification processes within the PV-PCM system, which operates continuously for 24 hours each day. The analytical approach significantly reduces computational time to a few seconds compared to over three months required by the CFD techniques. The transformation of the partial differential energy equation into a non-linear ordinary differential energy equation facilitates precise observation of both melting and solidification processes of the PCM material. The analytical approach is further applied to assess the performance of the PV-PCM system during two typical summer days in 2020 and 2021. Additionally, the impact of PCM thickness on the PV-PCM system is examined as a variable input. Tesults indicate that increasing PCM thickness from 1 cm to 5 cm reduces the peak temperature of the PV module by approximately 7 $^{\circ}C$. This temporal shift is significant, enabling the PV module to operate at cooler temperatures during peak solar intensity, resulting in higher power output. The analytical solution proves instrumental in determining the optimal PCM thickness for a PV-PCM system in any location within seconds. The findings reveal that a 5 cm PCM thickness leads to a 13% decrease in maximum temperature and a 3.4% increase in minimum electrical efficiency. The integration of thermal energy storage enhances the overall efficiency and performance of the PV system.

Keywords: *Analytical solution, Melting, PCM, Solar energy, Solidification, Thermal energy storage.*

1. Introduction

Solar energy has the greatest potential among all renewable technologies [1]. Photovoltaic (PV) modules have a widespread application because of their simplicity and low manufacturing cost compared to the other techniques of converting solar energy to electricity [2]. There are two main challenges in PV devices that the engineers are struggling with achieving higher efficiency and regulating their operating temperature [3]. Conventional first-generation solar cells have a relatively low efficiency ranging from 15% to 25% [4]. Hence, the third-generation multi-junction solar cells have been manufactured by scientists to achieve efficiency as high as around 47.1% under the AM1.5 spectrum [5]. According to Alexis De Vos [6], the theoretical maximum efficiency of tandem solar cells is 68% without any sunlight-concentrating devices. Although compound structure solar cells offer higher efficiency, there are still some barriers in the way to industrializing them such as being toxic to the environment, being fragile, and having a relatively low lifespan duration. On the other hand, first-generation solar cells' lifetime is over 25 years with a robust performance. Therefore, it is no surprise that in 2019 about 95% of PV panels available in the market belonged to first-generation solar cells [7]. Besides all the advantages single crystalline silicon cells possess, their electrical efficiency drops by elevating the operating temperature. To keep the PV temperature at a certain level, many researchers

have worked on different cooling systems for PV modules/panels.

Among various cooling methods, passive cooling techniques have lured the attention of the researchers because of benefits such as little maintenance cost [8] and zero-power consumption. This is in contrast to active cooling methods, where the cooling system consumes a fraction of PV power output. Passive cooling methods can be divided into six categories [9]:

a) Natural ventilation
b) Liquid immersion
c) Heat pipe
d) Thermoelectric generators
e) Phase change material (PCM)
f) Spectral beam splitter (SBS)

Each of the six techniques above has its attributes, and is utilized based on the specific application, geographical, and climatic conditions. The easiest and simplest one is natural ventilation, where the PV module/panel is cooled by natural air movement. However, it has the least impact on electrical efficiency improvement [8]. Liquid immersion has a higher heat transfer coefficient compared to air; consequently, immersing PV modules/panels under the water or floating them in the water will greatly decrease their temperature. Another option that could have a profound impact on regulating PV devices' temperature is the use of PCMs. PCMs have had extensive use in engineering fields such as air conditioning systems, water heating, cooling devices, and unnumbered industrial implementations [10]. The first use of PCMs in a PV module was done by Hausler *et al*. [11] in 1998. Starting from 2004 to 2011, Huang's research team pioneered the study of PV-PCM systems [12-14]. To tackle the problem of low thermal conductivity of PCMs, they have used aluminum extruded surfaces to enhance the heat transfer rate so that the PCM material was able to absorb more heat at a certain time. Aside from fins, there are other methods to enhance the effective thermal conductivity of PCMs including adding nanoparticles [15, 16], embedding a porous material with high thermal conductivity, and modification of geometrical and operational conditions. Concerning the geometrical aspect, Akshayveer *et al*. [17] have modified the conventional rectangular enclosure of a PCM, and achieved an 11.5% reduction in PV cell temperature. The incorporation of porous material with PCM could enhance the effective thermal conductivity of PCM up to more than 20 folds. Hence, many researchers have gone for metal foams, and studied the heat transfer performance of such devices. Recently, M. A. Essa *et al*. [18] studied the influence of porous metallic media (PMM) integrated with PCM on a PV module. Since water is circulated behind the PV module, their cooling system falls into active classification. Based on their experimental output, the PMM had superior performance compared to the system without PMM. Torsten Klemm *et al*. [19] numerically studied the heat transfer performance of PV-PCM system coupled with metallic fiber structure. They applied solar insolation as a function of time so that they were able to simulate the problem 24 hours a day. With a metallic fiber structure, the peak temperature of the PV module was decreased by about 20 K. M. A. Vaziri Rad [20] added an aluminum shavings porous media to a photovoltaic thermal (PVT) system. Their experimental setup was conducted in a cold and warm month starting from 9:30 to 17:00. At all times the PVT-PCM-Porous, PVT-PCM, PVT, and PV systems showed a better performance respectively. The reason behind the superior performance of the PVT-PCM-Porous system is the faster melting rate of the PCM in the vicinity of porous media. According to their report, by using porous media a 19%-25% reduction in the melting time of the PCM was observed. Although the combination of nanoparticles and PCMs has been extensively studied by the researchers, in terms of heat transfer, they are no match against fins or metallic porous media [21]. Therefore, in this study, extruded surfaces have been integrated with PCM to compensate poor heat transfer rate of a pure PCM.

In 2015, J. Zhou *et al*. [22] numerically analyzed the heat transfer performance of a silicon solar cell module (without a cooling system) at different radiation levels and ambient temperatures. They have mentioned that at higher radiation levels due to higher operating

temperatures, the conversion efficiency drops significantly. The wind speed was also considered in their study and reported that a 10 K temperature drop could be observed at 1000 $W/_{m^2}$ irradiation when wind speed is increased from 0 to 1 $m/_s$. Two years later, Tao Ma *et al*. [23], numerically studied the PV-PCM system performance for typical summer days in Shanghai. In their simulation, the ambient temperature, solar insolation, and wind speed were set as 30 $^{\circ}C$, 900 $W/_{m^2}$, and 4 $m/_s$, respectively. Subsequently, their simulations were performed for 360 minutes. Based on their outcome with the use of RT35HC PCM, the PV module temperature was maintained under 45 $^{\circ}C$ for 318 minutes. Another numerical study for concentrator PV-PCM systems was done by M. Emam and M. Ahmed [24] in the year 2018. In their cooling system, which the PCM heat sink consisted of parallel and series cavities, the results showed that increasing the number of parallel cavities led to further reduction of solar cell temperature, which was in contrast to increasing the series cavities. The reason is that by assembling the parallel cavities the heat is transferred from the solar cell to the back of the module, which has convective heat transfer boundary conditions via metal fins. However, in the series cavities, there are no metal fins that link the solar module to the back sheet, so increasing the number of series cavities will only result in higher resistance and lower heat transfer rate. While previously mentioned, papers considered a stable ambient condition; S. Khanna *et al*. [25] have studied the PV module performance under realistic climatic conditions. They were successful in simulating the PV module under climatic conditions of four different cities Madrid, Benidorm, Chennai, and Monaco. In their simulation, the ambient temperature and solar insolation vary with time, and a 24-hour full-day investigation has been done. One year after they optimized the PCM thickness and fin displacement under various working circumstances [26]. Parameters such as wind speed and wind azimuth effect have been considered on the PCM enclosure thickness. Unlike the other papers, the back sheet enclosure of the PCM material was set as an adiabatic condition. In real applications, a convective boundary condition is preferred since the PCM is being charged from the solar module side and discharged to the ambient from the other side. Hence, the PCM is under simultaneous charging and discharging (SCD) conditions, which may show a different behavior [27]. Regarding SCD conditions, J. M. Mahdi *et al*. [28] have paid attention to this matter so they added an exterior metal foam layer behind the PV-PCM system. With the exterior metal foam layer, the PCM melting time was extended by up to 32%-55%. Juan Duan [29] has also considered convective boundary conditions and simulated a concentrator PV-PCM system. A copper porous media has been used to enhance the effective thermal conductivity of the RT70HC PCM. The results convey that by decreasing the porosity the electrical efficiency could be increased. In another study, Juan Duan [30] experimentally and numerically studied the inclination angle effect on the PCM-porous cooling system of a PV module. He mentioned that by increasing the inclination angle the melting rate will increase.

In a recent scientific investigation by Xu *et al*. [31], the impact of Phase Change Material (PCM) on photovoltaic (PV) panels was explored through meticulous experiments. The indoor tests were conducted under an irradiation level of 1000 lux and an ambient temperature of 7.3 $^{\circ}C$. The PCM container affixed to the rear surface of the PV panel possessed a thickness of 30 mm. The findings demonstrated a noteworthy reduction of approximately 35 $^{\circ}C$ in the average temperature of the PV panel for 300 minutes. Maghrabie and colleagues [32] investigated the use of RT42 phase change material (PCM) to reduce the temperature of PV panels. Various PCM thicknesses, namely 1 cm, 2 cm, and 3 cm were affixed to the PV panel at different tilt angles, including 15°, 20°, 25°, and 30°. The most favorable outcome was observed at the 30° tilt angle. According to their findings, the electrical efficiency of the PV-PCM system increased by 14.4% in comparison to the standalone PV panel.

The literature review confirms that there is still a gap in the fast thermal analysis of a PV-PCM system under realistic environmental conditions. Under real environmental conditions, the solar insolation, ambient temperature, wind speed, etc. vary over time, so finding a suitable PCM enclosure thickness would be a challenging task that requires a deep study in this area. The experimental techniques would be time-consuming and pricey; the CFD technique also requires huge computational costs besides being a time-wasting method. The present paper aims to evaluate the minimum PCM thickness requirement by a novel analytical method that would be sufficient to absorb the excess heat of the PV module and also get solidified during nocturnal. This novel technique is based on writing the conservative energy equation for a PV-PCM system over time. To the best of the authors' knowledge, for the first time, this technique is applied to PV and PV-PCM systems to study their thermal behavior in real outdoor conditions. Although the outdoor realistic simulation has been performed concerning the coordinates of Babol city (36.53° N, 52.67° E), it is expected that the design procedure of the current study could be applied to any other case studies with different geographical and climatic conditions.

2. Problem description

The geometry of the present paper case study along with boundary conditions is well depicted in figure 1. Figure 1 (a) exhibits the 3D view of PV laminates' placement sequence on each other. The PV module size is considered to be $300\times300\ mm^2$, so that the 2D model view represents just a portion of the whole domain. Five aluminum plate fins have been added inside the PCM enclosure to maximize the heat transfer rate. The topological measurements accompanying with thermos-physical properties of the PV-PCM system have been represented in table 1. Since the simulation has been performed in both outdoor and indoor conditions, for the outdoor case the module is tilted about 36.53° degrees from horizontal, while in indoor conditions, the module is assumed to be mounted horizontally. The main goal of the current paper is to find a suitable PCM type with a minimum thickness required to be able to maintain the module temperature during the diurnal. Moreover, the fins' effect has also been paid attention to, hence, three different arrangements have been analyzed in indoor conditions, and the best arrangement has been chosen for real environmental conditions. These arrangements are shown in figure 2. It is worth noting that the fins' areas in all different arrangements are the same, so that for arrangement "C" since the length is twice of the other "A" and "B" arrangements the thickness is half (0.5 mm). It is also worth noting that the PV module is assumed to be a monocrystalline type with a reference efficiency of 20%. According to M. Mattei *et al*. [33], photovoltaic module efficiency is a linear function of its operating temperature, which could be defined as below:

$$\eta_{PV}=\eta_{ref}\left(1-\beta_{ref}\left(T_{cell\ layer}-T_{ref}\right)+0.085\ln\left(\frac{I_{solar}}{I_{ref}}\right)\right) \quad (1)$$

where I_{solar}, η_{ref}, β_{ref}, T_{ref}, and I_{ref} are the intensity of the solar insolation, the reference cell efficiency (%20 at 298.15 K), reference temperature coefficient (0.005 1/K), reference temperature (298.15 K), and reference solar intensity (1000 W/m^2), respectively [26]. From equation 1, it can be concluded that the efficiency of a PV module will drop as it gets heated so the power output of the PV module will decrease. This is not the only disadvantage of temperature rise in PV modules; according to O.O. Ogbomo *et al*. [34], the module fatigue life will decay exponentially with temperature. Thus regulating PV module temperature is vital during its lifetime.

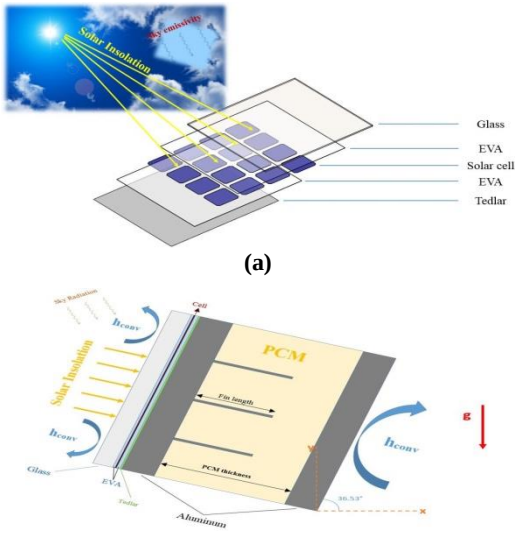

Figure1. (a) 3D representation of PV system, (b) 2D representation of PV-PCM system.

Table 1. The thermo-physical and optical properties of the PV system used in the current study [29].

Materials	Thickness [mm]	Density [kg/m^3]	Thermal conductivity [W/m.K]	Specific heat [J/kg.K]	
Glass	3.0	3000	2	500	
EVA	0.5	960	0.35	2070	
Cell	0.2	2330	148	677	
Tedlar	0.3	1200	0.2	1250	
Aluminum plates	5	2675	211	903	
	Absorptivity	Reflectivity	Transmissivity	Emissivity	Refractive index
Glass	0.04	0.04	0.92	0.9	1.526
EVA	0.08	0.02	0.9		1.45
Cell	0.9	0.08	0.02		3.69
Tedlar	0.13	0.86	0.012	0.9	1.45

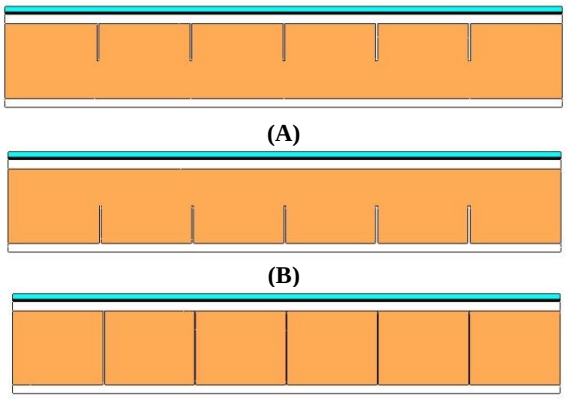

Figure 1. Three different fins arrangements in the PV-PCM system (A): Fins attached to the upper surface of the PV module, (B): Fins attached to the lower surface of the PCM container, (C): Fins embedded in the middle of the PCM container by attaching lower and upper surfaces

3. Model relations

3.1. Analytical method

The CFD simulation is an accurate method to estimate the operating temperature of the PV module alone or in the vicinity of a PCM material under realistic operating conditions, so that the peak temperature of the PV or PV-PCM system can be determined in 24 hours. Despite its precise forecast, it's a pretty time-consuming method; hence, it has been tried to find an alternative solution that could quickly yield the operating temperature of a PV module or PV-PCM system. Lumped system assumption considers a spatially uniform temperature, which would simplify the governing equations of the problem. Consequently, the problem is studied analytically considering the input and output of the energies. The lumped assumption is valid only if the Biot number is less than 0.1. With this regard, if the whole PV module is going to be modeled as lumped capacitance, its Biot number should be determined first. Equation (2) defines the Biot number relation:

$$Bi = \frac{h_c L_c}{k} \tag{2}$$

The effective thermal conductivity of the whole PV module needs to be determined. Accordingly, since the PV module layers are connected in series, the effective thermal conductivity of the whole system could be determined by writing the total conduction resistance equation:

$$R_{total} = R_{glass} + R_{EVA} + R_{cell} + R_{EVA} + R_{tedlar} \tag{3}$$

$$\frac{t_{PV}}{k_{eff,PV}} = \frac{t_{glass}}{k_{glass}} + \frac{t_{EVA}}{k_{EVA}} + \frac{t_{cell}}{k_{cell}} + \frac{t_{EVA}}{k_{EVA}} + \frac{t_{tedlar}}{k_{tedlar}} \tag{4}$$

Since the thickness of the PV module layers and their thermal conductivity are known, the PV module's effective thermal conductivity could be

obtained, which has a 0.76811 ($\frac{W}{m.K}$) value. The characteristic length of the PV module is considered as its total thickness of it (4.5 mm). Now the Biot number could be calculated at all times by substituting the forced convection heat transfer coefficient at different times. Figure 3 shows the Biot number over the whole computational duration which has less than 0.1 value at most times, which justifies the lumped assumption.

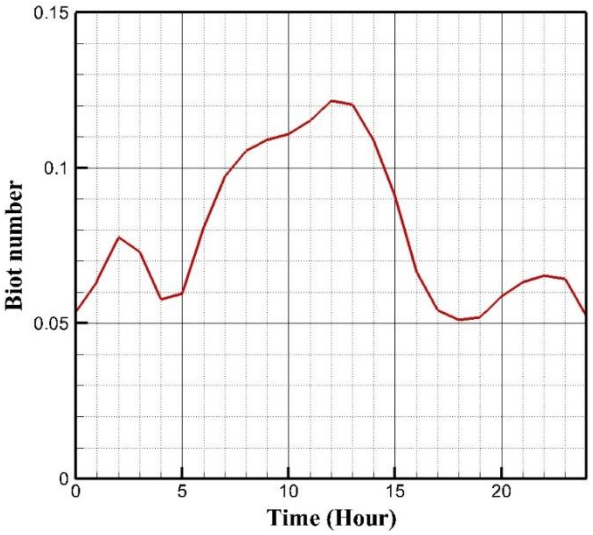

Figure 2. Biot number variation over time.

In the case of analytical analysis of the PV module, the conservation of energy equation would be written as:

$$\dot{E}_{in} - \dot{E}_{out} + \dot{E}_g = \dot{E}_{st} \tag{5}$$

where:

$\dot{E}_{in} = GA_s(1-r)$,

$\dot{E}_{out} = 1.5h_{c,\,force}A_s(T(t)-T_{amb}) + \varepsilon\sigma A_s(T(t)^4 - T_{sky}^4) + \varepsilon\sigma A_s(T(t)^4 - T_{amb}^4)$,

$\dot{E}_g = -0.2(1-0.005(T(t)-298.15))(0.828\times 0.9\times G\times A_s)$,

$\dot{E}_{st} = (m_{glass}C_{P,\,glass} + 2m_{EVA}C_{P,\,EVA} + m_{cell}C_{P,\,cell} + m_{tedlar}C_{P,\,tedlar})\frac{dT(t)}{dt}$,

and

$$G = \begin{cases} I_{solar} & 3025 \le t \le 55340 \\ 0 & otherwise \end{cases}$$

The analytical analysis has also been applied to the case of the PV-PCM system. This time, the governing equations will alter over time since the latent heat is added to the energy equation when PCM reaches the melting point. Therefore, depending on the geographical and ambient conditions the energy equation could be divided into a maximum of 5 piecewise equations varying over time. The governing energy equation of the PV-PCM system would be the same as equation (5); however, the term $\dot{E}_{st}$ is a piecewise function of the system's temperature, which could be followed as:

$$\dot{E}_{st} = \begin{cases} (m_{glass}C_{P,\,glass} + 2m_{EVA}C_{P,\,EVA} + m_{cell}C_{P,\,cell} + m_{tedlar}C_{P,\,tedlar} + m_{PCM}C_{PCM} + m_{fins}C_{al})\frac{dT(t)}{dt} & T < T_s \\ (m_{glass}C_{P,\,glass} + 2m_{EVA}C_{P,\,EVA} + m_{cell}C_{P,\,cell} + m_{tedlar}C_{P,\,tedlar} + m_{PCM}C_{PCM} + m_{fins}C_{al})\frac{dT(t)}{dt} + \Gamma m_{PCM}\frac{\partial\lambda}{\partial t} & T_s \le T \le T_l \\ (m_{glass}C_{P,\,glass} + 2m_{EVA}C_{P,\,EVA} + m_{cell}C_{P,\,cell} + m_{tedlar}C_{P,\,tedlar} + m_{PCM}C_{PCM} + m_{fins}C_{al})\frac{dT(t)}{dt} & T > T_l \end{cases} \tag{6}$$

In equation (6), the latent heat of PCM comes into action as soon as the system reaches the melting point. Hence, the stored energy would be a piecewise function of the system's operating temperature. The challenge of solving equation (5) for the case of the PV-PCM system is that the $\dot{E}_{st}$ term, as shown in equation (6), is not a single equation. Consequently, the code is divided into 5 sections, which are as follows:

1) Before the melting duration of PCM material
2) During the melting duration of PCM material (The latent heat is added to the equation)
3) After the melting duration of PCM material when PCM is fully melted
4) During the solidification of PCM material (The latent heat is added to the equation)
5) After the solidification duration of PCM material when PCM is fully solidified

Each section above has its unique equation with an initial temperature that is required to be determined by solving the energy equation of the previous section. For both PV and PV-PCM systems, the analytical solution is a non-linear ordinary differential equation (ODE), which has variable boundary conditions that are a non-linear

function of time. Due to the emissivity radiation heat transfer from the PV surface, the non-linearity of energy equation (5) is fourth order of magnitude. MAPLE software is used to solve the governing non-linear energy equations for both PV and PV-PCM systems.

3.2. Governing equations of CFD technique

The CFD technique has been used in this study for two main reasons:

1) To be compared with the analytical method
2) To find the best fin arrangement

Therefore, in this section, the governing equations applied to the PV-PCM system have been thoroughly discussed. Solar insolation is applied to the front (top) layer of the PV module, and penetrates to the other layers, gradually increasing its temperature and conducting the excess heat to the aluminum plate and the attached PCM after that. All three mechanisms of heat transfer such as radiation, convection, and conduction took place in the current study. To model the radiation through PV module layers discrete ordinate (DO) method is applied. In the DO radiation model, the intensity is considered as a function of $\vec{r}$ a position, and $\vec{s}$ as a direction vector, and then it is applied in equation (7) [35].

$$\nabla\cdot\left(I(\vec{r},\vec{s})\vec{s}\right)+(a+\sigma_s)I(\vec{r},\vec{s})=an^2\frac{\sigma T^4}{\pi}+\frac{\sigma_s}{4\pi}\int_0^{4\pi}I(\vec{r},\vec{s}')\,\phi(\vec{s},\vec{s}')d\Omega' \quad (7)$$

In the above equation, $\vec{s}'$, σ_s, σ, a, n, ϕ, and Ω' are scattering direction vector, scattering coefficient, Stefan-Boltzmann constant, spectral absorption coefficient, refractive index, phase function, and solid angle, respectively. The refractive index values of different module layers are taken from the reference [35]. The scattering phase function is assumed to be isotropic. The spectral absorption coefficient (a) is required to be determined, which is a function of the material thickness ($t_{thickness}$), transmissivity (τ), and reflectivity (r) [36]:

$$a=\left(\frac{1}{t_{thickness}}\right)\ln\left[\frac{(1-r)^2}{2\tau}+\sqrt{\frac{(1-r)^4}{4\tau^2}+r^2}\right] \quad (8)$$

Since all the unknowns of equation (7) are determined, the intensity could be calculated and applied as a source term in the conduction heat transfer equation of the PV module layers:

$$\frac{\partial(\rho_i C_{p_i} T_i)}{\partial t}=\nabla.(k_i\nabla T_i)-\gamma\dot{e}_{elec}+S_h \quad (9)$$

where "i" denotes the different PV module layers, the parameter "γ" obtains the value of one for the cell layer and zero for the other layers, and S_h is the source term related to the absorption of the radiation energy by each PV module layer, which could be determined if both radiation and energy equations are solved simultaneously.

$$S_h=-\nabla\cdot q^R=\nabla\cdot\int_0^{+\infty}q_v^R dv \quad (10)$$

where q_v^R the spectral radiative flux crossing a surface with a normal unit vector $\vec{n}$ is expressed as:

$$q_v^R=\vec{q}_v^R\cdot\vec{n}=\int_{4\pi}I_v\vec{n}\cdot\vec{s}d\Omega \quad (11)$$

The only unknown parameter of equation (9) is "$\dot{e}_{elec}$", which could be determined by equation (12):

$$\dot{e}_{elec}=\frac{E_{elec}}{V_{cell\ layer}}=\frac{(\alpha_{cell}\tau_{glass}I_{solar})\eta_{PV}}{t_{cell\ layer}} \quad (12)$$

where E_{elec}, $V_{cell\ layer}$, α_{cell}, τ_{glass}, $t_{cell\ layer}$, I_{solar}, and η_{PV} are the electrical power output of the PV module, the total volume of the cell layer, the absorptivity of the cell layer, the transmissivity of the glass layer, the thickness of the cell layer, the intensity of the solar insolation, the PV module efficiency, respectively.

In the case of a PV-PCM system, it is necessary to consider the continuum, momentum, and energy equations of the PCM material. Equation (13) below stands for the continuum equation of the PCM:

$$\nabla.V=0 \quad (13)$$

where "V" is the velocity vector in the Cartesian coordinate.

Equations (14 and 15) are the momentum equations of the PCM material in the Cartesian coordinate:

$$\frac{\partial u}{\partial t}+V.\nabla u=\frac{1}{\rho}\left(-\frac{\partial P}{\partial x}+\mu\nabla^2 u+\rho\beta g\cos\theta(T-T_{ref})\right)+S_u \quad (14)$$

$$\frac{\partial \upsilon}{\partial t}+V.\nabla \upsilon=\frac{1}{\rho}(-\frac{\partial P}{\partial y}+\mu\nabla^2\upsilon-\rho\beta g\sin\theta(T-T_{ref}))+S_v \quad (15)$$

The two source terms in the momentum equations are modeled as:

$$S_u=C(1-\lambda)^2\frac{u}{\lambda^3+\zeta} \quad (16)$$

$$S_\upsilon=C(1-\lambda)^2\frac{\upsilon}{\lambda^3+\zeta} \quad (17)$$

where C stands for mushy zone constant which is in the range of 10^5-10^6. In this study, the value of 10^5 is used as it has been recommended by several studies [37–40]. Moreover, the symbol ζ is added to the denominator to avoid division by zero.

Eventually, the energy equation of the PCM material is defined as:

$$\frac{\partial h}{\partial t}+\frac{\partial(\Delta H)}{\partial t}+\nabla.(Vh)=\nabla.\left(\frac{k}{\rho C_p}\nabla H\right) \quad (18)$$

The equations below represent the calculation of the sensible enthalpy of PCM and latent heat, respectively:

$$h=h_{ref}+\int_{T_{ref}}^{T}C_p dT \quad (19)$$

$$\Delta H=\lambda\Gamma \quad (20)$$

In the above equations, h_{ref} is the reference enthalpy of the PCM material at 273 K, C_p is the specific heat capacity of the PCM at constant pressure, and λ is the PCM liquid fraction term, which varies in the range of zero to one, and is described as:

$$\lambda=\begin{cases}0 & \mathrm{T}\le \mathrm{T}_s\\ (T-T_s)/(T_l-T_s) & \mathrm{T}_s<\mathrm{T}<\mathrm{T}_l\\ 1 & \mathrm{T}\ge \mathrm{T}_l\end{cases} \quad (21)$$

The advection movement of the PCM material because of the narrow temperature differences is considered and modeled as a Boussinesq approximation:

$$\rho=\rho_l(1-\beta(T-T_m)) \quad (22)$$

where ρ_l is the density of the PCM in the liquid form and T_m is defined as the average of solidus and liquidus temperatures of the PCM, $T_m=(T_s+T_l)/2$.

Since the PCM is trapped in an aluminum container with plate fins, the heat transfer equation inside the aluminum chamber and the fins is essential to be mentioned:

$$\frac{\partial(\rho_{Al}C_{p_{Al}}T_{Al})}{\partial t}=\nabla.(k_{Al}\nabla T_{Al}) \quad (23)$$

The thermo-physical properties of RT35-HC PCM used in this study are described in table 2 [41].

Table 2. The thermo-physical properties of the PCM used in this study [41].

Properties	RT35-HC
ρ (kg/m^3)	778.2
C_p (J/kgK)	2000
k (W/mK)	0.2
(kg/ms) μ	0.0044
(J/kg) Γ	220000
(K) T_s	307.65
(K) T_l	309.15
(1/K) β	0.000865

3.3. Governing equations of CFD technique

Initially ($t=0$), the PV-PCM system is at an ambient temperature (T_{amb}) lower than the PCM solidus temperature, so that the PCM is in the solid form. After that, the solar insolation is applied at the top layer of the PV module (glass) as a semitransparent medium along with external radiation sources (sky temperature for the outdoor condition and room temperature for the indoor case). While the side layers are assumed to be adiabatic and opaque the convection heat transfer is applied at the front and back layers. The heat transfer coefficient term for the outdoor condition is considered to be a linear function of wind speed and for the indoor case, the natural convection is regarded. Therefore, in the following paragraphs, the formulas of forced and natural heat transfer coefficients are studied.

Equations (24 and 25) present the natural convection heat transfer coefficient of horizontally positioned hot plates [42]:

$$h_{c,\,natural} = Nu\frac{k}{L} \quad \begin{matrix} Nu = 0.54Ra^{1/4} & 10^4 \le Ra \le 10^7 \\ Nu = 0.15Ra^{1/3} & 10^7 \le Ra \le 10^{11} \end{matrix} \quad \text{Hot surface be on top} \tag{24}$$

$$h_{c,\,natural} = Nu\frac{k}{L} \quad Nu = 0.27Ra^{1/4} \quad 10^5 \le Ra \le 10^{10} \quad \text{Hot surface be on the bottom} \tag{25}$$

where "L" is the characteristic length of the plate and is defined as the ratio of the surface area of the plate to its perimeter $L \equiv \frac{A_s}{Perimeter}$ and "Ra" is the Rayleigh number of external free convection flows:

$$Ra = \frac{g\beta(T_s - T_{amb})L^3}{\nu\alpha} \tag{26}$$

In the "Ra" equation, β, T_s, ν, and α stands for thermal expansion coefficient of air, plate surface temperature, air kinematic viscosity, and air thermal diffusivity. It is noteworthy to mention that all the aforementioned parameters are taken at air film temperature, which is the average temperature of the plate surface temperature and ambient temperature ($T_f \equiv \frac{T_s + T_{amb}}{2}$). Since the PV module front and bottom surfaces,' temperature needs to be known as "T_s" temperature, so that the air properties can be determined and the natural heat transfer coefficient be calculated; an initial value is guessed for the area-weighted average temperature of the PV module front and bottom layers, and subsequently, the heat transfer coefficient is applied as the boundary condition. Finally, the front and bottom surface temperatures obtained from the CFD simulation are compared with the approximate values and if the absolute error is less than %3 the calculated natural heat transfer coefficient would be fine.

Under outdoor circumstances, the forced heat transfer coefficient, ambient temperature, and solar insolation are all time-dependent variables. Hence, the NASA weather station [43] is used to get the hourly data of the variables on summer days (01/07/2021-02/07/2021), and then the variables are defined as a function of time. The forced heat transfer coefficient could be calculated as a linear function of wind speed as expressed below [44]:

$$h_{c,\,force} = 5.7 + 3.8V_w \tag{27}$$

Equation (27) is valid for wind speeds less than 5 m/s.

The sky temperature could be determined as a function of ambient temperature as demonstrated by [45]:

$$T_{sky} = 0.0522T_{amb}^{\,1.5} \tag{28}$$

A 24-hour simulation is performed based on the data available in table 3. Since the time step size for the CFD simulation is 0.1 seconds, the hourly data are converted to seconds, and then the variables' correlation against time is extracted and applied as variable boundary conditions. Equations (29-32) express the solar insolation, ambient temperature, sky temperature, and heat transfer coefficient as a function of time. It is worth mentioning that the heat transfer coefficient applied to the bottom side of the PV-PCM system is half of the front side which will be calculated from equation (27) as reported in [22].

$$I_{solar} = 0.272144657 \times (t/3600)^4 - 8.799134715 \times (t/3600)^3 + 74.74533917 \times (t/3600)^2 - 58.38249256 \times (t/3600) + 1.45981424 \tag{29}$$

$$h_{c,\,force} = -1.11825E-26 \times (t^6) + 2.8092E-21 \times (t^5) - 2.57601E-16 \times (t^4) + 1.03905E-11 \times (t^3) - 1.77582E-07 \times (t^2) + 0.001210806 \times t + 9.184282488 \tag{30}$$

$$T_{amb} = -1.33538E-22 \times (t)^5 + 3.0515E-17 \times (t)^4 - 2.35706E-12 \times (t)^3 + 6.46593E-08 \times (t)^2 - 0.000234058 \times (t) + 298.3721879 \tag{31}$$

$$T_{sky} = -1.8246E-22 \times (t)^5 + 4.16964E-17 \times (t)^4 - 3.22148E-12 \times (t)^3 + 8.84556E-08 \times (t)^2 - 0.000323948 \times (t) + 269.0417665 \tag{32}$$

Table 3. Hourly weather data of Babol City on summer days.

Hour	Solar Insolation (W/m^2)	Wind speed (m/s)	Time start (s)	T_{amb} (K)	T_{sky} (K)	Heat transfer coefficient (W/m^2K)
4	0	0.93	0	298.26	268.88	9.23
5	12.8	1.36	3600	297.99	268.51	10.86
6	113.5	1.99	7200	299.73	270.87	13.26
7	284.1	1.78	10800	301.12	272.75	12.46
8	474.4	1.09	14400	302.69	274.89	9.84
9	651.33	1.18	18000	304.34	277.14	10.18
10	791.58	2.14	21600	305.41	278.60	13.83
11	882.3	2.87	25200	306.14	279.60	16.60
12	930.17	3.24	28800	306.79	280.49	18.01
13	901.08	3.4	32400	307.4	281.33	18.62
14	814.65	3.48	36000	307.2	281.06	18.92
15	678.95	3.68	39600	306.73	280.41	19.68
16	507.25	3.96	43200	305.85	279.21	20.74
17	316.67	3.91	46800	304.34	277.14	20.55
18	138.3	3.39	50400	302.46	274.58	18.58
19	19.88	2.59	54000	300.52	271.94	15.54
20	0	1.49	57600	299.36	270.37	11.36
21	0	0.94	61200	299.02	269.91	9.27
22	0	0.8	64800	299.1	270.01	8.74
23	0	0.83	68400	298.9	269.74	8.85
0	0	1.14	72000	299.02	269.91	10.03
1	0	1.34	75600	298.96	269.82	10.79
2	0	1.44	79200	298.78	269.58	11.17
3	0	1.39	82800	298.61	269.35	10.98
4	0	0.85	86400	298.19	268.78	8.93

4. Results and discussion

Results from the study are presented and discussed based on two criteria: numerical simulation and analytical modeling. In the numerical simulation method, the geometry of the PV-PCM case study is designed and meshed. After that, boundary conditions are applied, and the governing equations are solved based on the finite element method. This method is accurate enough, yet possesses high computational cost. As

a consequence, an analytical approach is introduced to investigate the thermal performance of a PV or a PV-PCM system 24 hours round in just a few seconds. Therefore, with this approach, finding suitable PCM type and thickness would be rather easy for different environmental conditions.

4.1. Model validation

Both analytical and CFD methods have been compared with the experimental work of R. Ahmadi *et al*. [46] for stand-alone PV and PV-PCM systems. In the case of the CFD technique, the transient 2D numerical simulation of the PV module alone and PV-PCM system have been done by using the ANSYS Fluent software package. A SIMPLE scheme has been selected for pressure-velocity coupling. For spatial discretization of pressure, momentum, and energy, PRESTO, and QUICK options were selected respectively. The area-weighted average temperature of the glass layer has been computed over each time step and validated against experimental data. In the work of [46], a solar cell with a dimension of $5.5\times5.5\ cm^2$ is used for their experimental experiments. All their experiments were done under indoor conditions with a solar simulator. Hence, the natural convection heat transfer coefficient has been applied to the boundary condition. Figure 4 and figure 5 show the comparison of the present study with the experimental work of [46] under 800 W/m^2 irradiation for PV alone and PV-PCM systems respectively. From figure 4 and figure 5, can be understood that both the analytical method and CFD technique are in very good agreement with the experimental results. However, the CFD technique has about a 2% lower deviation compared to the analytical approach. From figure 5, it can be derived that when the PV temperature reaches 40 $^{\circ}C$; the increasing rate of it will be mitigated. The reason is that the PCM used in the work of [46] had a melting temperature range of 40-49 $^{\circ}C$. Other solar intensities have also been considered to compare the experimental results of [46] with the analytical approach. Figure 6 shows the stand-alone PV module temperature comparison of experimental and analytical techniques.

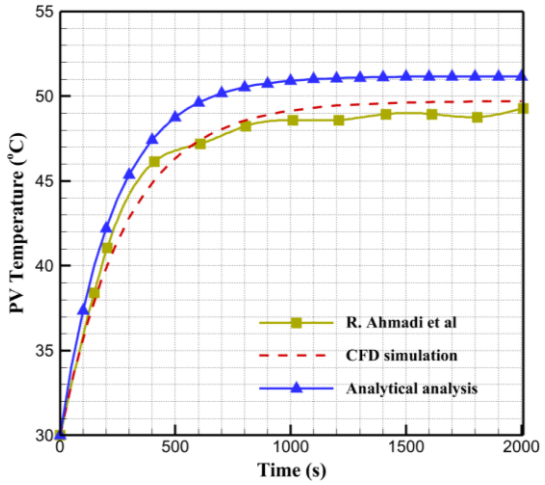

Figure 3. Comparison of analytical method with CFD simulation and experimental work of PV system of Ref. [46].

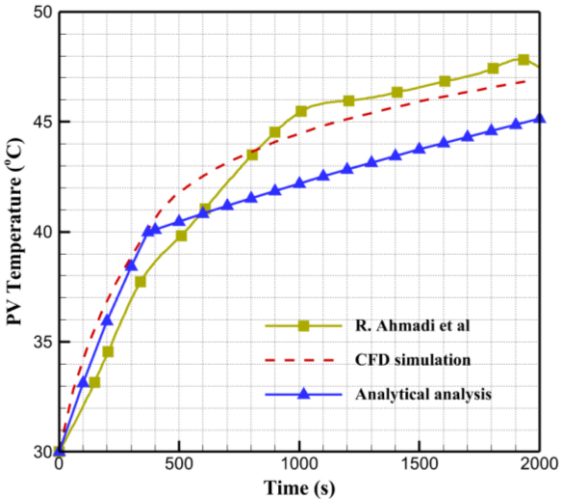

Figure 4. Comparison of analytical method with CFD simulation and experimental work of PV-PCM system Ref. [46].

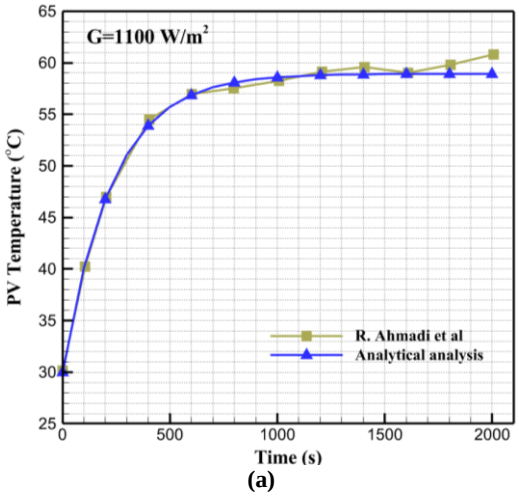

(a)

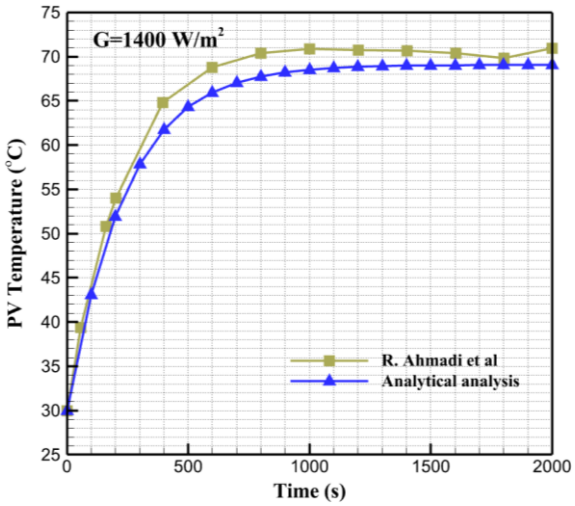

(b)

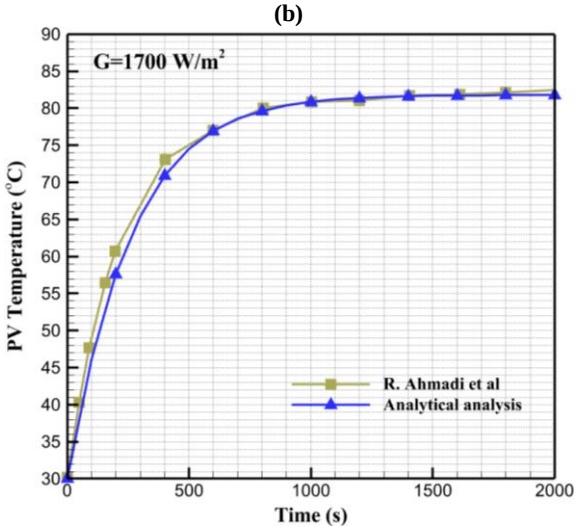

(c)

Figure. 5. Stand-alone PV module temperature comparison at intensity levels of (a) 1100 W/m^2 (b) 1400 W/m^2 (c) 1700 W/m^2.

To certify the analytical results of the current study with another experimental work whose PV dimensions are closer to our study, Huang *et al.* [12] research paper has been considered for comparison. In their specific study, it has been mentioned that the PV dimensions are $130\times300\ mm^2$ 40 mm PCM thickness. The paraffin wax PCM with 32 $^{\circ}C$ melting points was chosen for their specific experimental test and its other thermo-physical characteristics could be found in their paper. The insolation and ambient temperature were set as 750 W/m^2 and 21 $^{\circ}C$, respectively. Therefore, the PCM was fully solidified when the PV-PCM system was exposed to solar radiation. The PV module average temperature experimental results are compared with our analytical approach and summarized in figure 7. It can be seen that the analytical approach can follow the trend with a relatively good accuracy with maximum 12% error.

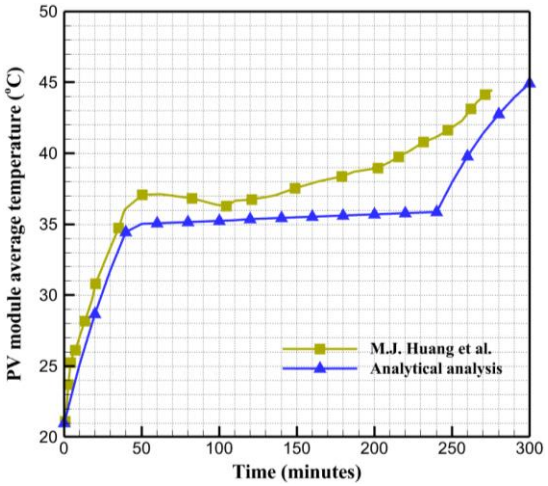

Figure. 6. Comparison of analytical method with experimental work of PV-PCM system Ref. [12].

Regarding a daily 24 hours of operation of a stand-alone PV system, the differential equation (5) is solved by MAPLE software for a typical summer day in Babol City, and the answer is astonishingly matched with the CFD simulation. Figure 8 shows the comparison of the two different methods for the same problem. Since the results obtained from the MAPLE programming are in very good agreement with the CFD simulation and computational cost is negligible, this method could be used to investigate a PV module/panel performance under realistic environmental conditions of any desirable location.

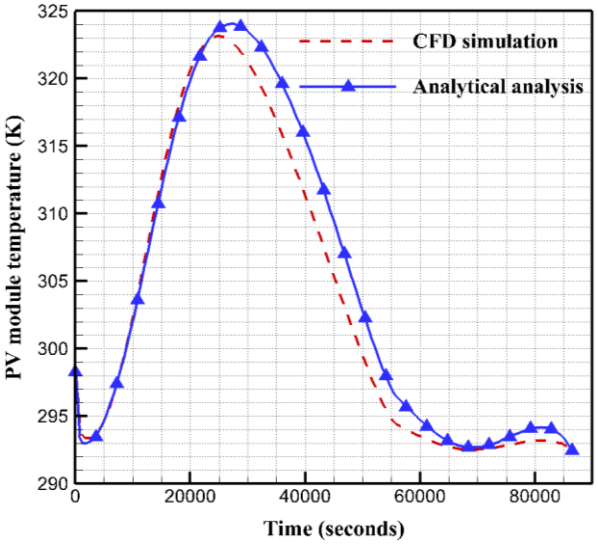

Figure. 7. Comparison of numerical CFD simulation with analytical method (lumped assumption).

4.2. Grid independence check of CFD technique

Since the area-weighted average temperature of the glass layer was the parameter chosen for validation, this parameter has also been used for

convergence criteria of different grid sizes. Table 4 holds the data related to the grid independence test. Since the data is not changing significantly from 82200 elements and above, the 82200 elements are assumed to be sufficient for the rest of the calculations. With a 58-core processor (Intel(R) Xeon(R) 2.60 GHz) and 96.0 GB RAM, which was used for simulation and post-processing, it took more than 3 months to do a 24-hour simulation of a PV-PCM system under realistic environmental conditions with 0.1 (s) time-step size.

Table 4. Grid size independence verification is based on the area-weighted average temperature of the glass layer of the PV module at different times.

Number of grids	0 (s)	300 (s)	600 (s)	900 (s)	1200 (s)
36400	298.15	305.294	309.286	310.529	311.007
54400	298.15	305.28	309.27	310.43	310.94
82200	298.15	305.28	309.27	310.41	310.92
96600	298.15	305.28	309.26	310.40	310.92

4.3. Effect of fins

The different fins' configurations shown in figure 2 are analyzed under constant irradiance (1000 W/m^2) and natural convection (indoor experiment). The goal is to find the best fin configuration under indoor conditions and then apply it to real outdoor environmental conditions by CFD technique. The reason that the outdoor condition is not applied to the problem is the simulation process, which would take a very long time for CFD analysis. From Figure 9, the comparisons between three different cases of "A", "B", and "C" could be done. It can be concluded that case "C" was able to keep the PV temperature at a lower rate compared to the other cases. Since cases "A" and "B" are hotter than case "C" by 22.4% and 33.5% after 5 hours of operation, this case has been chosen for further analysis. This conclusion can also be derived from Figure 10, where different cases' liquid fractions are compared. At the same boundary conditions, the faster the PCM is melted means more heat is absorbed from the PV module; hence, lower the PV temperature would be. Now that the best fin configuration has been revealed and chosen, the CFD technique and analytical approach could be compared under real outdoor conditions. This topic is discussed in the next paragraph. It is crucial to mention that the analytical method is not capable of comparing different fins arrangements, since the problem is solved by the Lump assumption which ignores the spatial temperature gradient.

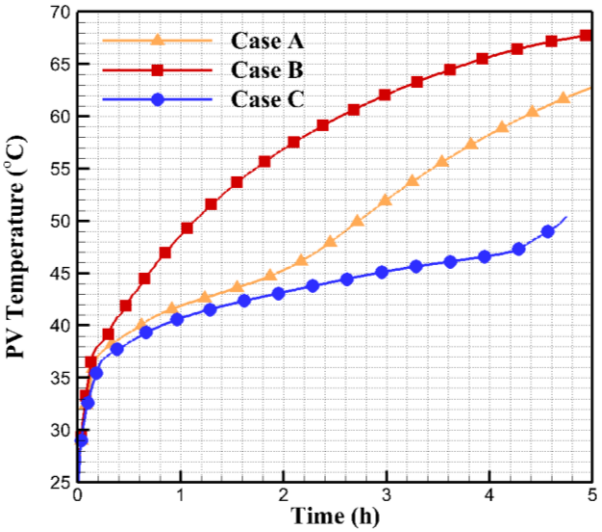

Figure 8. PV module temperature comparison of three different fin arrangements.

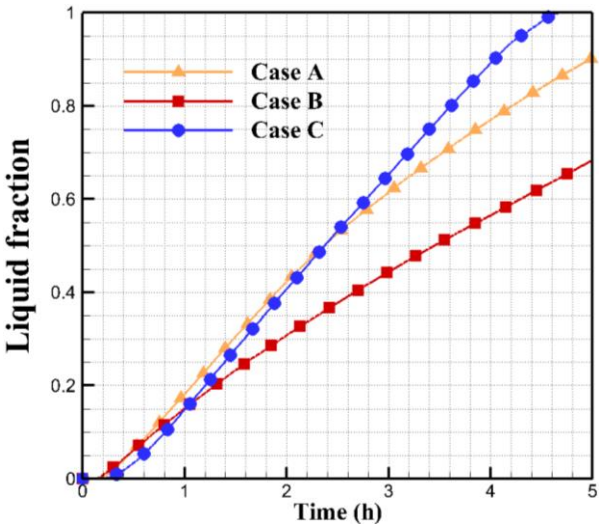

Figure 9. Liquid fraction comparison of three different fin arrangements.

The analytical and CFD results are compared with each other for a 10 mm PCM thickness with 5 plate fins inside the PCM domain under real environmental conditions of Babol City on July 1, 2021. From figure 11, it can be concluded that the analytical method could estimate the system's temperature with a reasonable accuracy. Subsequently, the analytical method is not only

accurate enough but also computationally it has no match since it takes less than a few seconds to be computed.

By carefully comparing the CFD simulation and analytical graphs, it could be concluded that the analytical method could not precisely evaluate the thermal performance of the system in the melting duration of the PCM. The cause of such discrepancy is due to the mixing heat transfer phenomena in the melting duration where both conduction and convection took place. The analytical method is incapable of computing the natural convection heat transfer inside the PCM. Figure 12 obtained from the CFD results shows the liquid fraction contours of the PV-PCM system between times 0-44100 seconds. From figure 12, the natural convection due to the buoyancy effect could be observed. In addition, the mixing heat transfer mechanism, which occurs between time 15300 (s) and 54000 (s) is revealed. A magnified portion of the PV-PCM system where streamlines are drawn shows the natural convection, which is rotating in a clockwise direction. The upper wall where the PV is attached is heated and the PCM is melted subsequently. A thin melted layer of PCM is shaped in the vicinity of the PV module and due to natural convection, it will slowly move upward. Figure 13 shows the solidification process of the PCM attached to the PV module. Similar to melting time, in solidification both conduction and convection are responsible for heat transfer. However, before melting time and after solidification the conduction is the dominant heat transfer so that the analytical method is perfectly matched with the CFD result.

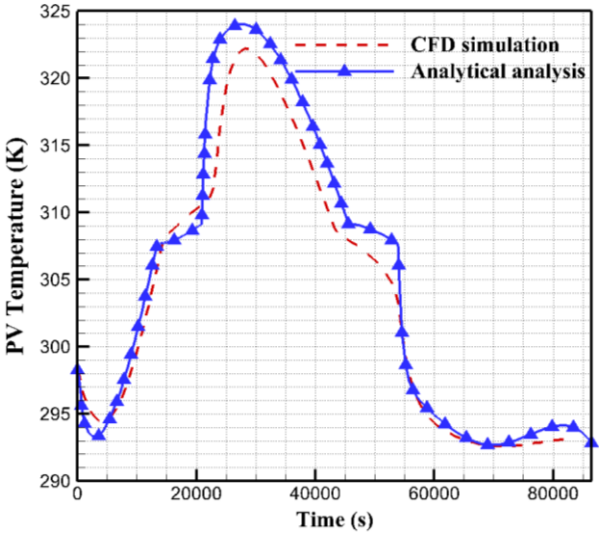

Figure 10. Results comparison of analytical analysis and CFD simulation of PV-PCM system with 10 mm PCM thickness and fins.

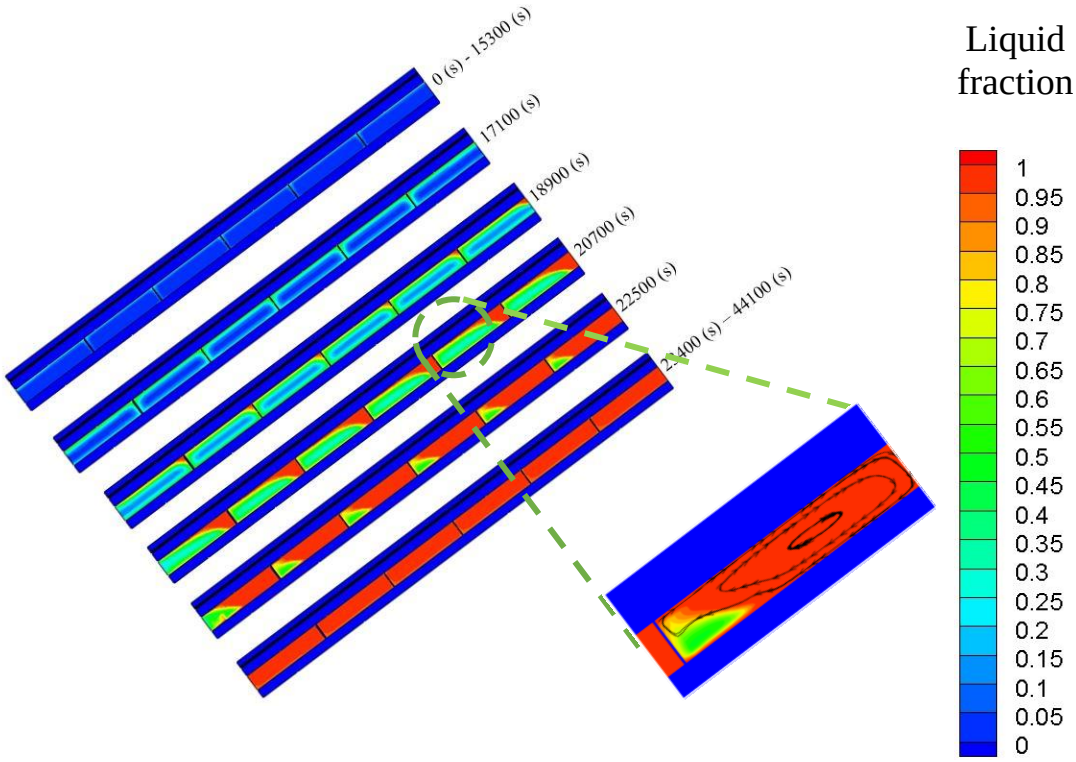

Figure 11. Melting procedure of PCM in the PV-PCM system.

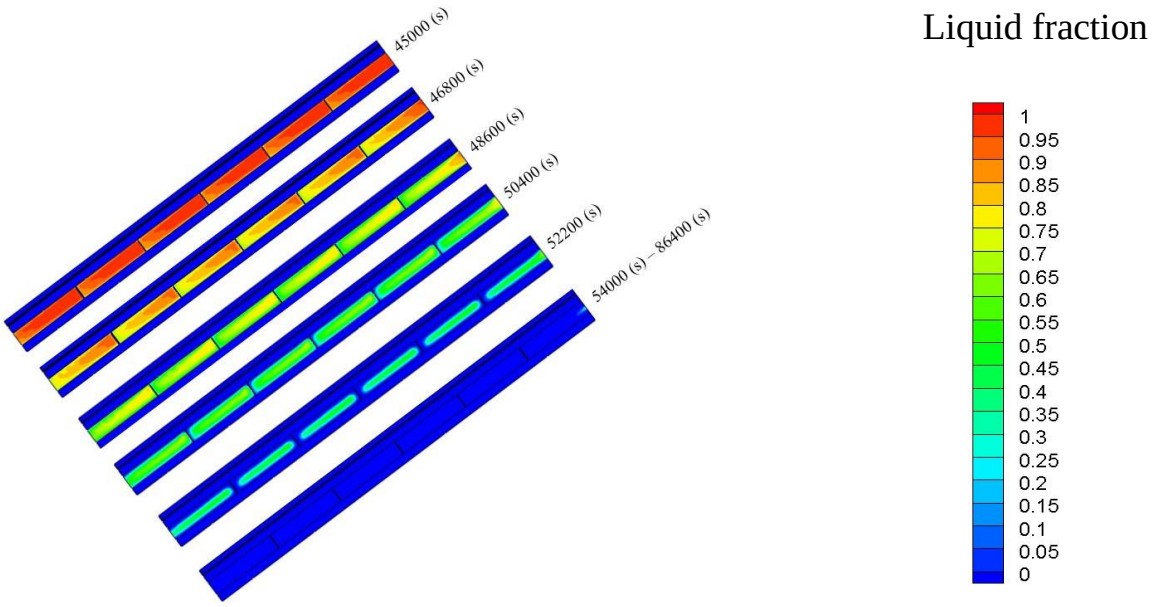

Figure 12. Solidification procedure of PCM in the PV-PCM system.

Since the temperature of the analytical solution and CFD results are slightly different from each other, in the melting and solidification duration of PCM material, the liquid fraction term has been compared between the phase-changing times of PCM. The results of both the CFD simulation and the analytical procedure are depicted in figure 14. It can be concluded that the two graphs follow a similar trend with a slight shift. This negligible difference is due to the spatial temperature gradient which is ignored in the analytical approach. In the analytical approach (lumped assumption), the whole system has a single temperature at any moment, while, in CFD simulation, it's possible to distinguish the temperature gradient from the hot surface (insolation side) to the cold surface (convection surface).

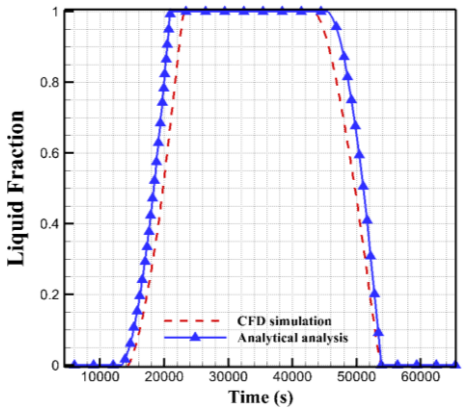

Figure 13. Comparison of analytical solution and CFD simulation in terms of liquid fraction.

4.4. Finding a suitable PCM thickness

The PV module attached to a PCM enclosure with 10 mm thickness is analyzed on a summer day in Babol City in Iran. To find out the passive cooling effect on the PV module performance during day and night the CFD simulation is applied for both PV stand-alone and PV-PCM systems. Subsequently, the module temperature with and without PCM cooling is compared. From figure 15, it can be concluded that with the PCM, the PV module temperature is kept at a lower level during peak sunshine hours. However, it will be increased dramatically after the PCM is fully melted. Since by increasing the PCM thickness, it would be possible to extend the melting duration and suppress the peak of the chart, different PCM thicknesses are compared with each other, and the results are presented in figure 16. From figure 16, it can be derived that with an increment in PCM thickness, the hill chart of PV temperature is firstly mitigated, and secondly shifted to the late sunshine hours. The peak temperature of the PV module is decreased by about 13.14% (6.69 $^{\circ}C$) by increasing the PCM thickness from 1 cm to 5 cm. Moreover, at all PCM thicknesses, the PCM would be solidified and ready for the next thermal cycle. It is requisite to mention that in figure 15 and figure 16, the "X" axis is the time duration which starts from 4:00 AM on 01/07/2021 and finishes at 4:00 AM on 02/07/2021.

In the analytical analysis, the whole PV and PCM systems are considered as a united system;

afterwards, the conservation of energy equation is written for it. In the aforesaid scenario, the cell temperature is defined as PV-PCM temperature, whereas, in the CFD simulation it was possible to report the cell layer temperature at a defined time step interval. Figure 17 compares the electrical efficiency value of the PV module for two different systems of PV and PV-PCM. From figure 17 it can be inferred that the efficiency drop of the PV module in the vicinity of a PCM would be shifted to a later time, hence, the PV module will operate with higher efficiency at peak sunshine hours.

Although the use of PCMs for cooling PV modules/panels possesses a lot of advantages, they are still not justifiable economically. Therefore, researchers need to find new methods to decrease the amount of PCM usage or decrease the total cost of PCM materials. Nevertheless, PCMs could be a viable cooling method in space applications where the rate of cooling is low due to being limited to radiation only.

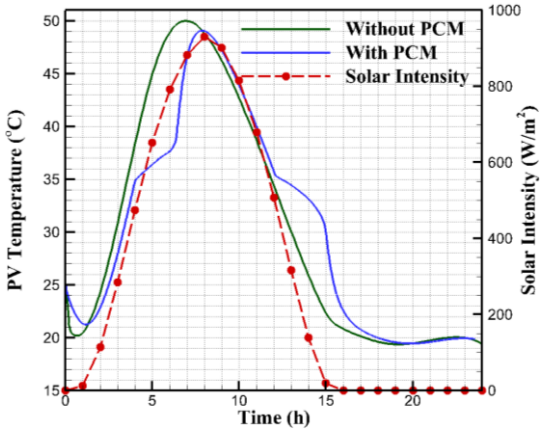

Figure 14. The PV module temperature comparison with and without PCM.

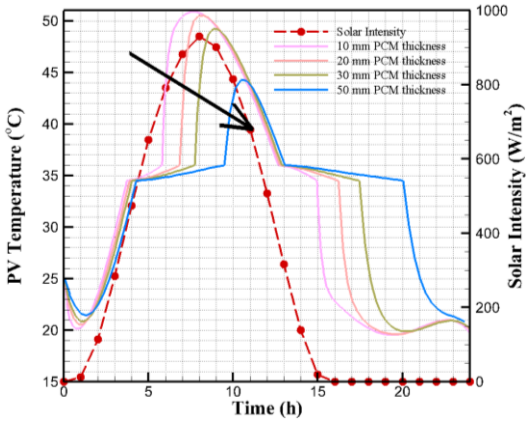

Figure 15. PV module temperature against different PCM thicknesses.

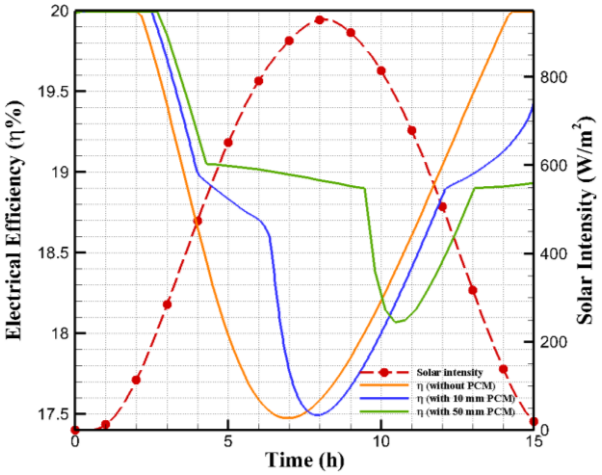

Figure 16. Electrical efficiency versus time duration starting from 4:00 AM.

Another study has been done regarding the thermal performance of the PV-PCM system on a summer day in 2020. The main difference between this study with the previous one is the ambient temperature and wind speed values. In 2020, the wind speed was roughly twice that of 2021 with lower ambient temperature. The solar insolation intensity of both summer days of 2020 and 2021 was about the same. Figure 18 is prepared to make the comparison of these boundary conditions easier. For this scenario, both CFD simulation and analytical approach have been done. Since both results' discrepancy was negligible, once again the analytical method has been verified. Figure 19 shows the comparison of the thermal performance of two different methods. From figure 19, it can be derived that the hill chart of the PV temperature plot has been flattened, and the PCM used behind the PV system was not fully melted. Because of the higher wind speed, the heat transfer coefficients that have been applied as boundary conditions were higher. This resulted in flattening the hill chart of the PV temperature plot. This outcome is important since, with a 10 mm PCM thickness applied behind the PV module, the system is perfectly cooled for the case of a 2020 summer day. However, for the case of the 2021 summer day, the hill chart could be observed. Therefore, it is necessary to apply the analytical code for all months to analyze the PV-PCM performance under different environmental conditions and then find the optimum PCM thickness requirement which would be suitable for a relatively long period of a year.

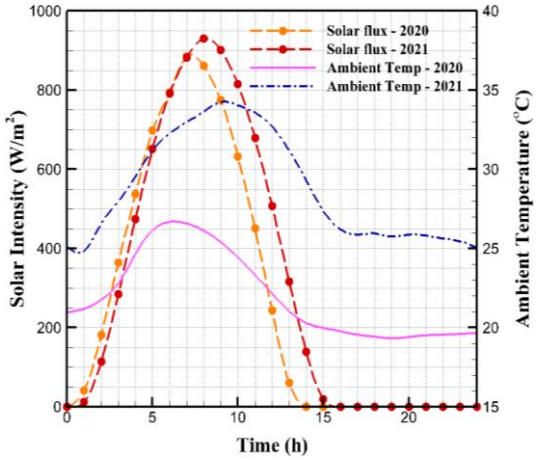

(a)

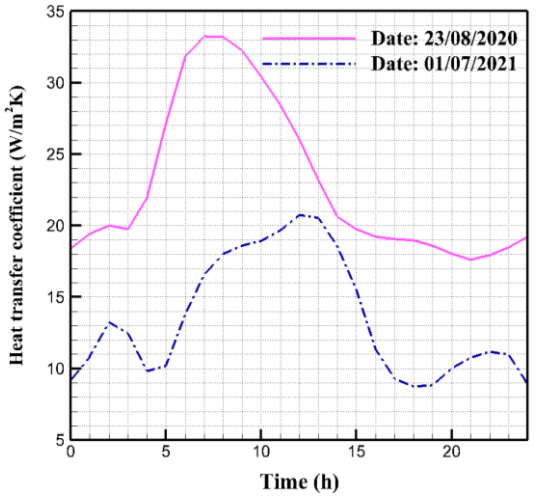

(b)

Figure 17. Boundary conditions of two different summer days (2020 and 2021).

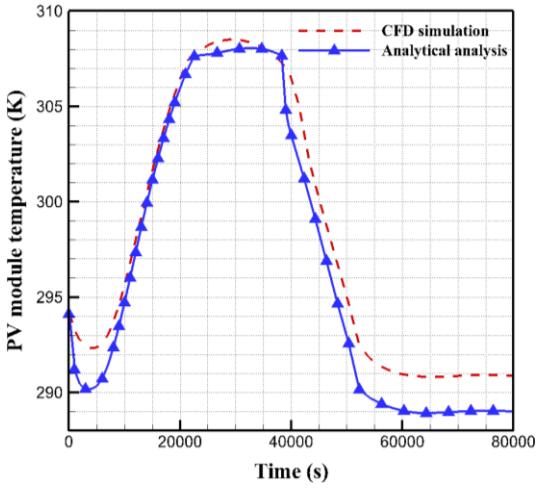

Figure 18. Results comparison of analytical analysis and CFD simulation of PV-PCM system with 10 mm PCM thickness and fins.

Figure 20 is depicted to compares the PV module temperature and efficiency of the two different summer years. Since the maximum temperature of the PV module on a typical summer day in 2021 reaches 51 $^{\circ}C$, which is 16 $^{\circ}C$ higher than another typical summer day in 2020; it has led to an 8% decrease in the minimum efficiency. If the average values of PV module efficiency of the different case studies are calculated over time when solar flux is not zero for the years 2020 and 2021, 19.52% and 18.98% will be yielded. The enormous difference between the results of two consecutive years will make this result clarify that even though the energy input (solar intensity) is almost the same for the two cases, two other parameters such as wind speed and ambient temperature are game-changers. Therefore, it is strongly recommended to install PV modules/panels in an open windy area where there are no obstacles so that a higher heat transfer coefficient will be applied.

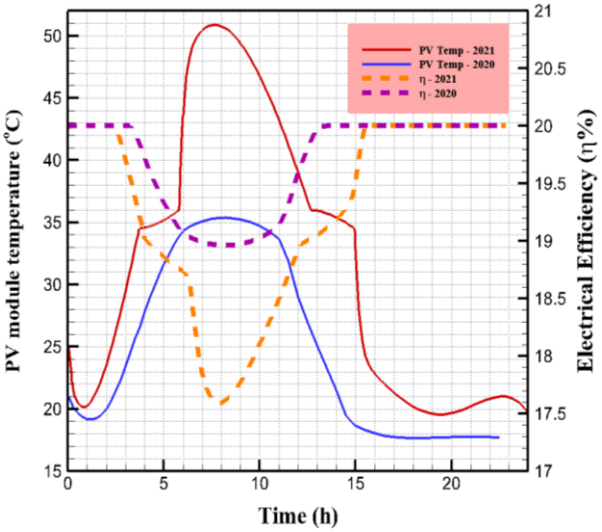

Figure 19. PV temperature and efficiency in the vicinity of a 10 mm PCM in different summer years.

5. Conclusion

Concerning the widespread application of PCM with PV devices as a clean, renewable source of energy, many researchers have focused on the PCM cooling effect on a PV module. They have tried to calculate the amount of PCM requirement by usual CFD techniques which requires a lot of time. In this study, it has been tried to solve the problem by an analytical solution with lump assumption simplification, which alters the partial differential energy equation to a non-linear ordinary differential equation. It has been shown that with the CFD technique, it took more than 3 months to fully simulate the heat transfer process in the PV-PCM system for a 24-hour analysis; whereas, with an analytical approach the

computational time is less than a second. The results showed that the analytical solution successfully followed the CFD data with reasonable accuracy in a very short time. This achievement could be very useful for future software engineers to estimate the PV/PV-PCM system temperature and design process as well as optimization procedures where time is an important factor. Another noteworthy point of this study is the addition of fin materials to the PCM container to enhance the heat transfer rate for both melting and solidification processes. The analytical solution was successful in simulating the effect of fin materials within the PCM. This is a very good achievement since the analytical approach could be applied to other engineering topics with faster techniques of designing.

Regarding the accuracy of the analytical solution, the maximum deviations that have been seen between experimental and analytical results for the case of PV and PV-PCM systems were 3.79% and 5.73%, respectively. The analytical method could accurately follow the trend of PV or PV-PCM temperature in 24 hours of operation within a few seconds of calculation time. It could be applied at different locations with various environmental conditions which vary as a function of time. For Babol City on July 1, 2021, the analytical results showed that with 5 cm PCM thickness it was possible to decrease the maximum temperature by about 13% and increase the minimum electrical efficiency by 3.4%.

6. Nomenclature

Bi	Biot number
C	Mushy zone constant (kg m^{-3} s^{-1})
C_p	Specific heat (J kg^{-1} K^{-1})
g	Acceleration of gravity (m s^{-2})
h	Sensible specific enthalpy (J kg^{-1})
H	Total specific enthalpy (J kg^{-1})
I	Radiation intensity (W m^{-2})
P	Pressure (Pa)
T	Temperature (K)
T_l	Liquidus temperature (K)
T_s	Solidus temperature (K)
t	Time (s)
V	Fluid velocity vector (m s^{-1})
x, y	Cartesian coordinates (m)

7. Greek symbols

α	Thermal diffusivity (m^2 s^{-1})
a	Spectral absorption coefficient (m^{-1})
σ	Stefan-Boltzmann constant (5.67×10^{-8} W m^{-2} K^{-4})
n	Refractive index
β	Thermal expansion coefficient (K^{-1})
φ	Volume fraction
λ	Liquid fraction
μ	Dynamic viscosity (kg m^{-1} s^{-1})
ν	Kinematic viscosity (m^2 s^{-1})
ρ	Density (kg m^{-3})
ε	Emissivity
ζ	Small parameter for avoiding division by zero
Γ	Latent heat of fusion (J kg^{-1})
r	Reflectivity
τ	Transmissivity
ϕ	Phase function
Ω'	Solid angle
η	Electrical efficiency

8. Subscripts

amb	Ambient
c, conv	Convection
g	Generate
ref	Reference
st	Store

9. Abbreviations

CFD	Computational Fluid Dynamics
EVA	Ethylene-vinyl acetate
DO	Discrete ordinate
PCM	Phase Change Material
PV	Photovoltaic
PVT	Photovoltaic thermal
PMM	Porous Metallic Media
SBS	Spectral beam splitter
SCD	Simultaneous charging and discharging

10. References

[1] Nazir, Muhammad Shahzad, Amin Shahsavar, Masoud Afrand, Müslüm Arıcı, Sandro Nižetić, Zhenjun Ma, and Hakan F. Öztop. "A comprehensive review of parabolic trough solar collectors equipped with turbulators and numerical evaluation of hydrothermal performance of a novel model." Sustainable Energy Technologies and Assessments 45 (2021): 101103.

[2] Wang, Rong, Sandra Hasanefendic, Elizabeth Von Hauff, and Bart Bossink. "The cost of photovoltaics: Re-evaluating grid parity for PV systems in China." Renewable Energy (2022).

[3] Abdallah, Abdulhadi, Richard Opoku, Charles KK Sekyere, Samuel Boahen, Kofi O. Amoabeng, Felix Uba, George Y. Obeng, and Francis K. Forson. "Experimental investigation of thermal management techniques for improving the efficiencies and levelized cost of energy of solar PV modules." Case Studies in Thermal Engineering (2022): 102133.

[4] Kazem, Hussein A., Miqdam T. Chaichan, Ali HA Al-Waeli, and K. Sopian. "A review of dust accumulation and cleaning methods for solar photovoltaic systems." Journal of Cleaner Production (2020): 123187.

[5] https://www.nrel.gov/pv/cell-efficiency.html.

[6] De Vos, Alexis. "Detailed balance limit of the efficiency of tandem solar cells." Journal of Physics D: Applied Physics 13, No. 5 (1980): 839.

[7] Photovoltaics Report – Fraunhofer ISE, 2020. https://www.ise.fraunhofer.de/content/dam/ise/de/documents/publications/studies/Photovoltaics-Report.pdf.

[8] Ma, Tao, Zhenpeng Li, and Jiaxin Zhao. "Photovoltaic panel integrated with phase change materials (PV-PCM): technology overview and materials selection." Renewable and Sustainable Energy Reviews 116 (2019): 109406.

[9] Mahdavi, Arash, Mousa Farhadi, Mofid Gorji-Bandpy, and Amirhoushang Mahmoudi. "A review of passive cooling of photovoltaic devices." Cleaner Engineering and Technology (2022): 100579.

[10] Mahdavi, Arash, Mohammad Amin Erfani Moghaddam, and Davood Domiri Ganji. "Hierarchical implementation of hybrid heat promoters fixated on operational conditions to accelerate the melting phenomenon of a triplex tube heat exchanger." Thermal Science and Engineering Progress 25 (2021): 101008.

[11] Häusler, Tobias, and Harald Rogaß. "Photovoltaic module with latent heat-storage-collector." In 2nd World Conference on Photovoltaic Solar Energy Conversion, proceedings of the international conference held at Vienna, Austria, 6-10 July 1998, Vol. 1, pp. 315-317. Office for Official Publications of the European Communities, 1998.

[12] Huang, M. J., P. C. Eames, and B. Norton. "Thermal regulation of buildingintegrated photovoltaics using phase change materials." International Journal of heat and mass transfer 47, No. 12-13 (2004): 2715-2733.

[13] Huang, M. J., P. C. Eames, and Brian Norton. "Comparison of predictions made using a new 3D phase change material thermal control model with experimental measurements and predictions made using a validated 2D model." Heat Transfer Engineering 28, No. 1 (2007): 31-37.

[14] Huang, M. J., P. C. Eames, Brian Norton, and N. J. Hewitt. "Natural convection in an internally finned phase change material heat sink for the thermal management of photovoltaics." Solar Energy Materials and Solar Cells 95, No. 7 (2011): 1598-1603.

[15] Selimefendigil, Fatih, and Hakan F. Öztop. "Analysis of hybrid nanofluid and surface corrugation in the laminar convective flow through an encapsulated PCM filled vertical cylinder and POD-based modeling." International Journal of Heat and Mass Transfer 178 (2021): 121623.

[16] Rostami, Sara, Masoud Afrand, Amin Shahsavar, M. Sheikholeslami, Rasool Kalbasi, Saeed Aghakhani, Mostafa Safdari Shadloo, and Hakan F. Oztop. "A review of melting and freezing processes of PCM/nano-PCM and their application in energy storage." Energy 211 (2020): 118698.

[17] Kumar, Amit, Ajeet Pratap Singh, and O. P. Singh. "Effect of novel PCM encapsulation designs on electrical and thermal performance of a hybrid photovoltaic solar panel." Solar Energy 205 (2020): 320-333.

[18] Essa, Mohamed A., M. Talaat, Abdalla Amer, and M. A. Farahat. "Enhancing the photovoltaic system efficiency using porous metallic media integrated with phase change material." Energy 225 (2021): 120299.

[19] Klemm, Torsten, Abdelhakim Hassabou, Amir Abdallah, and Olaf Andersen. "Thermal energy storage with phase change materials to increase the efficiency of solar photovoltaic modules." Energy Procedia 135 (2017): 193-202.

[20] Rad, Mohammad Amin Vaziri, Alibakhsh Kasaeian, Soroush Mousavi, Fatemeh Rajaee, and Amir Kouravand. "Empirical investigation of a photovoltaic-thermal system with phase change materials and aluminum shavings porous media." Renewable Energy 167 (2021): 662-675.

[21] Xiong, Teng, Long Zheng, and Kwok Wei Shah. "Nano-enhanced phase change materials (NePCMs): A review of numerical simulations." Applied Thermal Engineering 178 (2020): 115492.

[22] Zhou, Jicheng, Qiang Yi, Yunyun Wang, and Zhibin Ye. "Temperature distribution of photovoltaic module based on finite element simulation." Solar Energy 111 (2015): 97-103.

[23] Ma, Tao, Jiaxin Zhao, and Zhenpeng Li. "Mathematical modelling and sensitivity analysis of solar photovoltaic panel integrated with phase change material." Applied Energy 228 (2018): 1147-1158.

[24] Emam, Mohamed, and Mahmoud, Ahmed. "Cooling concentrator photovoltaic systems using various configurations of phase-change material heat sinks." Energy conversion and management 158 (2018): 298-314.

[25] Khanna, Sourav, K. S. Reddy, and Tapas K. Mallick. "Effect of climate on electrical performance of finned phase change material integrated solar photovoltaic." Solar Energy 174 (2018): 593-605.

[26] Khanna, Sourav, Sanjeev Newar, Vashi Sharma, K. S. Reddy, and Tapas K. Mallick. "Optimization of fins fitted phase change material equipped solar photovoltaic under various working circumstances." Energy conversion and management 180 (2019): 1185-1195.

[27] Mahdavi, Arash, Mohammad Amin Erfani Moghaddam, and Amirhoushang Mahmoudi. "Simultaneous charging and discharging of multi-tube heat storage systems using copper fins and Cu nanoparticles." Case Studies in Thermal Engineering 27 (2021): 101343.

[28] Mahdi, Jasim M., Rupinder Pal Singh, Hussein M. Taqi Al-Najjar, Sukhmeet Singh, and Emmanuel C. Nsofor. "Efficient thermal management of the photovoltaic/phase change material system with innovative exterior metal-foam layer." Solar Energy 216 (2021): 411-427.

[29] Duan, Juan. "A novel heat sink for cooling concentrator photovoltaic system using PCM-porous system." Applied Thermal Engineering 186 (2021): 116522.

[30] Duan, Juan. "The PCM-porous system used to cool the inclined PV panel." Renewable Energy 180 (2021): 1315-1332.

[31] Xu, Zhiming, Qinglu Kong, Hongwei Qu, and Chong Wang. "Cooling characteristics of solar photovoltaic panels based on phase change materials." Case Studies in Thermal Engineering 41 (2023): 102667.

[32] Maghrabie, Hussein M., A. S. A. Mohamed, Amany M. Fahmy, and Ahmed A. Abdel Samee. "Performance enhancement of PV panels using phase change material (PCM): An experimental implementation." Case Studies in Thermal Engineering 42 (2023): 102741.

[33] Mattei, Michel, Gilles Notton, Christian Cristofari, Marc Muselli, and Philippe Poggi. "Calculation of the polycrystalline PV module temperature using a simple method of energy balance." Renewable energy 31, No. 4 (2006): 553-567.

[34] Ogbomo, Osarumen O., Emeka H. Amalu, N. N. Ekere, and P. O. Olagbegi. "Effect of operating temperature on degradation of solder joints in crystalline silicon photovoltaic modules for improved reliability in hot climates." Solar Energy 170 (2018): 682-693.

[35] Maadi, Seyed Reza, Meysam Khatibi, Ehsan Ebrahimnia-Bajestan, and David Wood. "Coupled thermal-optical numerical modeling of PV/T module–Combining CFD approach and two-band radiation DO model." Energy conversion and management 198 (2019): 111781.

[36] Hassanien, Ahmed Saeed, and Alaa A. Akl. "Effect of Se addition on optical and electrical properties of chalcogenide CdSSe thin films." Superlattices and Microstructures 89 (2016): 153-169.

[37] Seddegh, Saeid, Xiaolin Wang, and Alan D. Henderson. "A comparative study of thermal behaviour of a horizontal and vertical shell-and-tube energy storage using phase change materials." Applied Thermal Engineering 93 (2016): 348-358.

[38] Yuan, Yanping, Xiaoling Cao, Bo Xiang, and Yanxia Du. "Effect of installation angle of fins on melting characteristics of annular unit for latent heat thermal energy storage." Solar Energy 136 (2016): 365-378.

[39] Ye, Wei-Biao, Dong-Sheng Zhu, and Nan Wang. "Numerical simulation on phase-change thermal storage/release in a plate-fin unit." Applied Thermal Engineering 31, no. 17-18 (2011): 3871-3884.

[40] Kousha, N., M. J. Hosseini, M. R. Aligoodarz, R. Pakrouh, and R. Bahrampoury. "Effect of inclination angle on the performance of a shell and tube heat storage unit–An experimental study." Applied Thermal Engineering 112 (2017): 1497-1509.

[41] Faden, Moritz, Andreas König-Haagen, Stephan Höhlein, and Dieter Brüggemann. "An implicit algorithm for melting and settling of phase change material inside macrocapsules." International Journal of Heat and Mass Transfer 117 (2018): 757-767.

[42] Bergman, Theodore L., Adrienne S. Lavine, Frank P. Incropera, and David P. DeWitt. Introduction to heat transfer. John Wiley & Sons, 2011.

[43] https://power.larc.nasa.gov/data-access-viewer/.

[44] Sharples, S., and P. S. Charlesworth. "Full-scale measurements of wind-induced convective heat transfer from a roof-mounted flat plate solar collector." Solar Energy 62, no. 2 (1998): 69-77.

[45] Swinbank, W. CQJR. "Long-wave radiation from clear skies." Quarterly Journal of the Royal Meteorological Society 89, No. 381 (1963): 339-348.

[46] Ahmadi, Rouhollah, Farhad Monadinia, and Mahdi Maleki. "Passive/active photovoltaic-thermal (PVT) system implementing infiltrated phase change material (PCM) in PS-CNT foam." Solar Energy Materials and Solar Cells 222 (2021): 110942.